CrossMark

Proteomic identification of fat-browning markers in cultured white adipocytes treated with curcumin

Sang Woo Kim[2,3] · Jae Heon Choi[1] · Rajib Mukherjee[1] · Ki-Chul Hwang[2,3] ·
Jong Won Yun[1]

Abstract We previously reported that curcumin induces browning of primary white adipocytes via enhanced expression of brown adipocyte-specific genes. In this study, we attempted to identify target proteins responsible for this fat-browning effect by analyzing proteomic changes in cultured white adipocytes in response to curcumin treatment. To elucidate the role of curcumin in fat-browning, we conducted comparative proteomic analysis of primary adipocytes between control and curcumin-treated cells using two-dimensional electrophoresis combined with MALDI-TOF-MS. We also investigated fatty acid metabolic targets, mitochondrial biogenesis, and fat-browning-associated proteins using combined proteomic and network analyses. Proteomic analysis revealed that 58 protein spots from a total of 325 matched spots showed differential expression between control and curcumin-treated adipocytes. Using network analysis, most of the identified proteins were proven to be involved in various metabolic and cellular processes based on the PANTHER classification system. One of the most striking findings is that hormone-sensitive lipase (HSL) was highly correlated with main browning markers based on the STRING database. HSL and two browning markers (UCP1, PGC-1α) were co-immunoprecipitated with these markers, suggesting that HSL possibly plays a role in fat-browning of white adipocytes. Our results suggest that curcumin increased HSL levels and other browning-specific markers, suggesting its possible role in augmentation of lipolysis and suppression of lipogenesis by trans-differentiation from white adipocytes into brown adipocytes (beige).

Keywords Anti-obesity · Curcumin · Fat-browning · Proteome · White adipocytes

Abbreviations

2-DE	Two-dimensional electrophoresis
ANXA2	Annexin A2
AMPK	AMP-activated protein kinase
ATP5B	ATP synthase subunit beta, mitochondrial
CA3	Carbonic anhydrase 3
CS	Citrate synthase
C/EBP/*Cebp*	CCAAT/enhancer-binding protein/ encoding gene
FABP4	Fatty acid binding protein 4
HADH	Trifunctional enzyme subunit alpha
HSL	Hormone-sensitive lipase
HSP90	Heat shock protein 90 kDa
PGC-1α	Peroxisome proliferator-activated receptor gamma co-activator 1-alpha
MDH	Malate dehydrogenase
PPAR	Peroxisome proliferator-activated receptor
PRDM16/ *Prdm16*	PR domain-containing 16/encoding gene
UCP/*Ucp*	Uncoupling protein/encoding gene
WAT	White adipose tissue

✉ Sang Woo Kim
kimsw@daegu.ac.kr

✉ Jong Won Yun
jwyun@daegu.ac.kr

1 Department of Biotechnology, Daegu University, Kyungsan, Kyungbuk 712-714, Republic of Korea

2 Catholic Kwandong University, International St. Mary's Hospital, Incheon Metropolitan City 404-834, Republic of Korea

3 Institute for Bio-Medical Convergence, College of Medicine, Catholic Kwandong University, Gangneung-si, Gangwon-do 210-701, Republic of Korea

Introduction

Obesity is associated with disorders such as hypertension, dyslipidemia, endothelial dysfunction, and diabetes [1, 2]. It is mainly characterized by excessive deposition of adipose tissues, and induction of lipolysis is considered as a targeted therapy for the prevention and improvement of obesity [3, 4]. White adipose tissue (WAT) stores excess energy as triacylglycerol (TG) during fasting, and plays a key role in energy metabolism by providing free fatty acids (FFA) and glycerol through hydrolysis of TG [5]. In contrast, brown adipose tissue (BAT) is specialized for non-shivering thermogenesis through fat burning and high expression of mitochondrial uncoupling protein 1 (UCP1), which uncouples respiration and dissipates chemical energy as heat [6, 7].

Intriguingly, rediscovery of BAT in adult humans has led to a renaissance in the study of this tissue as a target for the development of therapeutic treatments for obesity [8]. Besides classical brown adipocytes, beige or "brite" (brown in white) adipocytes are developmentally distinct and are formed from transdifferentiation of mature white adipocytes or differentiation of brown adipogenic progenitors [9, 10]. Transcriptional regulators important for controlling expression of the BAT phenotype include PRDM16, PGC-1α, and PPARγ [9]. Among them, PGC-1α controls mitochondrial biogenesis and heat production by inducing expression of UCP1 and other respiratory factors. Most studies on induced browning of white adipocyte have been conducted under cold exposure and pharmacological activation of β3-adrenergic receptors in WAT via promotion of WAT remodeling by adipocyte progenitors [11, 12].

Meanwhile, there has been considerable investigation of pharmacological nutritional/dietary agents as well as signaling pathways that contribute to browning of WAT [13]. Several dietary compounds such as capsaicin, berberine, orexin, and irisin have been reported as browning promoters by energy expenditure and lipolysis [14–16]. Here, we focused on curcumin, a natural compound extracted from rhizomes of *Curcuma* species, since it is a naturally occurring curcuminoid of turmeric, which is a member of the ginger family (*Zingiberaceae*) [17]. Moreover, dietary curcumin administration was reported to prevent weight gain and play an anti-inflammatory role in obesity [18]. Our previous study indicated that curcumin along with a browning cocktail could synergistically induce the brite phenotype and drive BAT thermogenesis through significant elevation of brown fat-specific genes [19].

For comprehensive understanding of the role of adipose tissue in obesity, several proteomic studies using rodent adipose tissues have been carried out, and proteins in BAT and WAT from rodents subjected to high fat diet have been compared [20, 21]. Furthermore, comparative proteomic analysis was also carried out during brown preadipocyte differentiation or adipose tissue lipolysis [22, 23]. These studies demonstrated several mechanistic pathways that control expression of thermogenesis proteins in BAT. Previously, we reported that the expression of several thermogenic and lipogenic proteins varies in adipose tissues of obese prone and obese-resistant rats [20]. Another research group compared expression of proteins in WAT and BAT between calorie-restricted and control rats [24]. The results showed that ATP-citrate synthase (ACLY) was up-regulated by caloric restriction, which altered activities of proteins associated with energy metabolism.

In this study, we observed that curcumin has a browning effect on white adipocytes based on its ability to alter expression of brown adipocytes marker proteins in white adipocytes, thereby inducing acquisition of BAT features. To obtain more detail, we performed comparative proteomic analysis of primary white adipocytes between control and curcumin-treated adipocytes, as curcumin and a browning cocktail synergistically induced the brite phenotype. In addition, network analyses suggested that enhanced expression of HSL and other browning-specific markers by curcumin treatment reduces body fat by increasing lipolysis and suppressing lipogenesis by trans-differentiation from white adipocytes into beige adipocytes.

Materials and methods

Culture and differentiation of primary white adipocytes

Ten-day-old sprague-dawley (SD) rats were purchased from Daehan Experiment Animals (Seoul, Korea). Rats were used for isolation of primary stromal vascular fractions (SVFs) from rat inguinal fat pads, cultured, and differentiated into mature primary adipocytes as described previously [25]. In brief, inguinal fat pads were minced with scissors and digested with type I collagenase (1 mg/ml; Sigma-Aldrich) at 37 °C in a water bath shaker. After 90 min, contents were immediately filtered in mesh and centrifuged at $1000 \times g$ for 10 min. The layer of floating cells was then washed three times with PBS. Adipocytes were incubated in Dulbecco's modified Eagle's medium (DMEM) supplemented with 10 % FBS and 100 units/ml of penicillin–streptomycin (Sigma-Aldrich) under a 5 % CO_2 atmosphere at 37 °C. After reaching confluence (day 1), cells were initiated for adipocyte differentiation by incubation with differentiation-inducing medium consisting of 10 µg/ml of insulin (Sigma,

St. Louis, MO, USA), 0.25 μM dexamethasone (Sigma), and 0.5 mM 3-isobutyl-1-methylxanthine (IBMX, Sigma) in DMEM, followed by maturation medium containing 10 % FBS and 10 μg/ml of insulin. During treatments, unless otherwise stated, cells were maintained in complete medium containing 20 μM curcumin for 6–8 days before further analysis, and maturation medium was changed every 2 days. The range of curcumin doses (1–20 μM) used in this study was determined based on previous reports [19, 26]. For induction of adipocyte browning, differentiation-inducing medium was supplemented with 50 nM triidothyronine, whereas maturation medium was supplemented with 50 nM triidothyronine and 1 μM rosiglitazone (browning cocktail).

Preparation of protein samples for two-dimensional electrophoresis (2-DE)

Cells were lysed in 200 μL of rehydration buffer solution containing 7 M urea, 2 M thiourea, 4 % CHAPS, 20 mM DTT, 1 mM PMSF, 2 % IPG buffer (Ampholyte 3/10, Bio-Rad), and a trace of bromophenol blue. Lysed tissues were then homogenized by a homogenizer (PT 1200E, Kinematica, Luzern, Switzerland) on ice, after which extracts from homogenized WAT were centrifuged at $13,000 \times g$ for 20 min. The supernatant was then stored at -80 °C until analysis. Protein content of cells was determined using RC DC^{TM} protein assay (Bio-Rad).

2-DE

2-DE was performed in duplicate using protein samples from rat primary white adipocytes, which consisted of control and curcumin-treated cells. 2-DE experiments were conducted using previous methods outlined by our laboratory [20, 27, 28]. Briefly, immobilized pH gradient (IPG)-isoelectric focusing (IEF) of WAT samples was performed on pH 3–10, 18 cm IPG DryStrips (GE Healthcare, Buckinghamshire, UK) in a PROTEIN IEF cell (Bio-Rad) using the protocol recommended by the manufacturer. IPG strips were rehydrated passively for 12 h in strip holders with 350 μL of rehydration solution, which included 7 M urea (Bio Basic, Ontario, Canada), 2 M thiourea (Sigma, St. Louis, MO, USA), 4 % CHAPS (Bio Basic), 1 mM PMSF (Sigma), 20 mM DTT (GE Healthcare), 2 % IPG buffer (Bio-Rad), and 150 μg of primary white adipocyte proteins. IEF was executed as previously described [28]. Gel strips were then placed onto a 20×20 cm 12 % polyacrylamide gel for resolution in the second dimension. Fractionation was performed using the Laemmli SDS discontinuous system at a constant voltage of 15 mA per gel for 14 h. For image analysis and peptide mass fingerprinting (PMF), a total of six gels, including two gels per group with separated proteins, were visualized by silver staining [28].

Image acquisition and data analysis

Gels were imaged on a UMAX PowerLook 1120 (Maxium Technologies, Akron, OH, USA), and modified Image-Master 2-D software V4.95 (GE Healthcare) was used for comparison of images. A reference gel was selected from gels of the control group, and detected spots from other gels were matched with those in the reference gel. Relative optical density and relative volume were calculated in order to correct differences in in-gel staining. Each spot intensity volume was processed by background subtraction and total spot volume normalization, and the resulting spot volume percentage was used for comparison.

Protein identification

For protein identification by PMF, protein spots were excised, digested with trypsin (Promega, Madison, WI, USA), mixed with CHCA in 50 % ACN/0.1 % TFA, and subjected to MALDI-TOF analysis (Microflex LRF 20, Bruker Daltonics). Spectra were collected from 300 shots per spectrum over an m/z range of 600–3000 and calibrated by two-point internal calibration using trypsin auto-digestion peaks (m/z 842.5099, 2211.1046). Peak list was generated using Flex Analysis (ver 3.0). The threshold used for selecting peaks was executed as previously described [28]. Protein score is $-10 \times$ Log (p), where p is the probability that the observed match is a random event, and greater than 61 is significant ($p < 0.05$).

Immunoblot analysis

Cell lysates were prepared using RIPA buffer (Sigma) by homogenization and centrifugation at $14,000 \times g$ for 20 min. Immunoblot analyses were performed as previously described [28]. Briefly, the membrane was rinsed three times consecutively with TBS-T buffer, followed by incubation for 1 h with 1:500–1000 dilutions of primary monoclonal antibodies against ANXA2, ATP5B, HSP90, CA3, MDH, β-actin, PPARγ, p-AMPK, and HSL (1:200–500, Santa Cruz Biotechnology) in TBS-T buffer containing 1 % skim milk. After three washes, the membrane was incubated for 1 h with horseradish peroxidase-conjugated anti-goat IgG or anti-rabbit IgG secondary antibody (1:1000, Santa Cruz Biotechnology) in TBS-T buffer containing 1 % skim milk. Development was carried out using enhanced chemiluminescence (West Zol, iNtRON Biotechnology). Quantification of band intensities was performed by using ImageJ software (NIH).

Network analysis

For gene/protein classification and network analysis, identified proteins obtained from proteomic analysis together with major fatty acid metabolic proteins were analyzed using the Protein ANnotation THrough Evolutionary Relationship (PANTHER) and Database for Annotation, Visualization, and Integrated Discovery (DAVID) classification systems [29, 30]. These public databases allow the systematic division of large gene lists in an attempt to assemble a summary of related biological functions, pathways, and protein classes. DAVID provides a comprehensive set of functional annotation tools to understand the biological relevance of such a large list of genes/proteins. Identification of gene enrichment categories was carried out according to SP-PIR keywords combining the annotation from both Swiss-Prot (SP) and Protein Information Resource (PIR). Associations of differentially expressed genes/proteins with broadly defined molecular networks were combined and visualized using the STRING database.

Real-time RT-PCR

Transcription levels of genes were quantitatively determined by real-time RT-PCR (Stratagene Mx 3000p QPCR System, Santa Clara, CA, USA). Total RNA was isolated from WAT tissues using an easy-spin TM (DNA-free) Total RNA Extraction kit, and reverse-transcription was carried out using a Maxime RT Premix kit (iNtRON Biotechnology). FastStart Universal SYBR Green Master (Roche Diagnostics, Indianapolis, IN, USA) was employed for real-time RT-PCR. Transcription levels of each gene (*Acca2*, *Atp5b*, *Atp5h*, *Cebpb*, *Cs*, *Fabp4*, *Gpd*, *Hadha*, *Hspd1*, *Hspe1*, *Lipe*, *Mdh2*, *Ppard*, *Pparg*, *Ppargc1a*, *Prdm16*, *Ucp1*, *Ucp2*, *Ucp3*, and *Vdac1*) were normalized to *Gapdh* transcription levels, and relative changes in gene expression were quantified using the $\Delta\Delta C_T$ method [31]. Oligonucleotide sequences of the primers used are shown in Table 1.

Co-immunoprecipitation (Co-IP)

To identify UCP1/PGC-1α-interacting partner proteins in primary white adipocytes in response to curcumin treatment, Co-IP was performed with slight modifications as outlined in our laboratory [32]. Primary white adipocytes containing 500 µg of protein were incubated with 15 µl of anti-UCP1/PGC-1α antibody (Santa Cruz Biotechnology) at 4 °C for 3 h on a rotary shaker, after which 20 µl of A/G PLUS agarose conjugate suspension (Santa Cruz Biotechnology) was added and allowed to mix at 4 °C for 12 h on a rotary shaker. After centrifugation at $4000 \times g$ for 5 min at 4 °C, the supernatant was collected and the beads washed three times with RIPA buffer (Sigma). Then, $2 \times$ Laemmli buffer was added and boiled for 5 min. For the negative control sample, control rabbit IgG (Santa Cruz Biotechnology) was used. After Co-IP, all samples were separated by 8–12 % SDS-PAGE, after which samples were transferred to a PVDF for immunoblot analysis.

Statistical analysis

All experimental results were compared by One-way Analysis of Variance (ANOVA) using the Statistical Package of Social Science (SPSS, version 17) program; data are expressed as the mean ± SEM. A protected least-significant difference (LSD) test, which is a method for multiple comparison consisting of single-step procedures in One-way ANOVA, was used to demonstrate significant differences between means ($p < 0.05$).

Results

Proteomic analysis and classification of rat primary white adipocyte proteome

For identification of differentially expressed proteins between control (CN) and curcumin-treated adipocytes, all protein samples were separated by 2-DE (Fig. 1a) and identified by MALDI-TOF–MS (Table 2), and database searches were performed with high confidence based on high score and sequence coverage using MASCOT server. A total of 325 individual matched spots ranging in mass from 6 to 240 kDa between pH 3-10 were detected. Fifty-eight spots were identified with statistically different intensities between the CN and CR groups. These differentially altered spots showed dramatic alterations in response to curcumin treatment, suggesting that curcumin possibly plays a pivotal role in obesity prevention and lipolysis in primary white adipocytes. Next, differentially expressed proteins identified from the two groups were subjected to functional analysis using the PANTHER database. Functional analysis classified the identified proteins as related to biological processes, molecular function, and protein class by PANTHER classification (Fig. 1b). These proteins were involved in metabolic processes (50 %), cellular processes (18.1 %), and localization (12.5 %) based on GO Biological Process. These proteins were also involved in catalytic and transporter activities based on GO Molecular Function. In PANTHER Protein Class, identified proteins were classified as oxidoreductase (24.5 %), hydrolase (14.3 %), cytoskeletal protein (8.2 %), transferase (8.2 %), and chaperone (8.2 %). Among the differentially expressed spots, 25 spots were significantly

Table 1 List of primers for RT-PCR used in this study

Genes		Primer sequence (5′–3′)		
Acca2	F	AGAGGTGGAAAGCCGCTAAC	R	CTGTGACCGTCCCCTCTTTC
Atp5b	F	CCAAGGGTGGGAAAATCGGA	R	GGTCCTCTCACCAACACCAG
Atp5h	F	CCAGCGATTGACTGGGCTTA	R	CCTCAGGCACAGGGATCTTC
Cebpb	F	CAAGCTGAGCGACGAGTACA	R	CAGCTGCTCCACCTTCTTCT
Cs	F	TGCATGGACTAGCAAACCAG	R	ATATCCTGGGACAACCCGTC
Fabp4	F	AGAAGTGGGAGTTGGCTTCG	R	ACTCTCTGACCGGATGACGA
Gpd	F	TGGGCTTGAGAGTGAGGTTGC	R	GCCACCGTTTTCCAGTCACA
Hadha	F	GGGAATCTTACCAGGAGCCG	R	TGCTCTGTCTGCACGAATGT
Hspd1	F	CTCACTCGCCGCAGACG	R	CACTGGTCTCATCTGGCGAA
Hspe1	F	ACACGGAGGCACCAAAGTAG	R	AGTGGAATGGGCAGCTTCAT
Lipe	F	TCCCTGTACCACAGCAATCA	R	AGCTGGAGGTGGTTCTGCT
Mdh2	F	GACCCAGCTCGAGTCAATGT	R	CCTTCACGACTTCAGTGCCA
Ppard	F	AGGACATGAGCCATCCAAAG	R	TACACCCCTTCCCTTCAGTG
Pparg	F	CCCTGGCAAAGCATTTGTAT	R	ACTGGCACCCTTGAAAAATG
Ppargc1a	F	ATGTGTCGCCTTCTTGCTCT	R	ATCTACTGCCTGGGGACCTT
Prdm16	F	AGAGGATGAGGAACCACCCA	R	AAATGCTTCCTCAGCTGCTCT
Ucp1	F	AATCAGCTTTGCTTCCCTCA	R	GCTTTGTGCTTGCATTCTGA
Ucp2	F	GCAGTTCTACACCAAGGGCT	R	GGAAGCGGACCTTTACCACA
Ucp3	F	TGGCCTCTACGACTCTGTCA	R	CTCCAGTTCCCAGGCGTATC
Vdac1	F	GTCACCGCCTCCGAGAAC	R	CACTTTGGTGGTCTCCGTGT
Internal control				
Gapdh	F	ATCCCAACTCAGCCCCCAAC	R	ATGGTATTCGAGAGAAGGGAGGGC

F sequence from sense strands, *R* sequence from anti-sense strands

down-regulated, whereas 33 spots were up-regulated in curcumin-treated adipocytes (Fig. 2).

Differential expression of proteins involved in lipid metabolism and mitochondrial biogenesis

Prior to comparison of differentially altered proteins between the CN and CR groups, we classified proteins based on DAVID bioinformatics resources. To identify enriched functional gene groups in DAVID, identified proteins were converted from a UniProt protein ID into a DAVID gene ID. Candidate proteins were classified according to gene ontology entries in UniProt. After submitting the converted list into DAVID, top affected gene functions in curcumin-treated adipocytes were related to a central role in mitochondrial metabolism (Fig. 3a). Fourteen (ACCA2, ACO2, ALDH2, ATP5B, ATP5H, CS, DLD, GLUD1, HADHA, HSPD1, HSPE1, MDH2, PRDX5, and VDAC1) proteins were mainly localized to mitochondria and were shown to exert a variety of mitochondrial functions; proteins required for transport or transfer of fatty acids or proteins involved in lipid metabolism were observed frequently. DAVID analysis showed

that three (ALDH2, ATP5B, PRDX5) out of 14 proteins were down-regulated in adipocytes by curcumin treatment, whereas ATP5B expression was elevated by Western blot analysis. In functional pathway analysis by DAVID, two proteins (ACCA2 and HADHA) were shown to be involved in fatty acid degradation in mitochondria from the KEGG database (Fig. 3b). This process includes three major steps as follows: (1) lipolysis of and release from adipose tissue; (2) activation and transport into mitochondria; and (3) β-oxidation. Fatty acid degradation is the process in which fatty acids are broken down into their metabolites as the main energy supply of animals. Fatty acids must be activated before they can be transported to mitochondria for fatty acid oxidation.

To elucidate interactions between the identified proteins and brown fat-specific markers in primary white adipocytes, six proteins associated with fatty acid metabolism and mitochondrial function were verified by Western blot analysis (Fig. 4a). Two mitochondrial proteins (ATP5B (*Atp5b*) and MDH (*Mdh2*)) were significantly up-regulated in response to curcumin treatment, whereas expression of HSP90 was reduced. Two fatty acid metabolic proteins (HSL (*Lipe*) and CA3) were significantly up-regulated in primary white adipocytes with curcumin treatment,
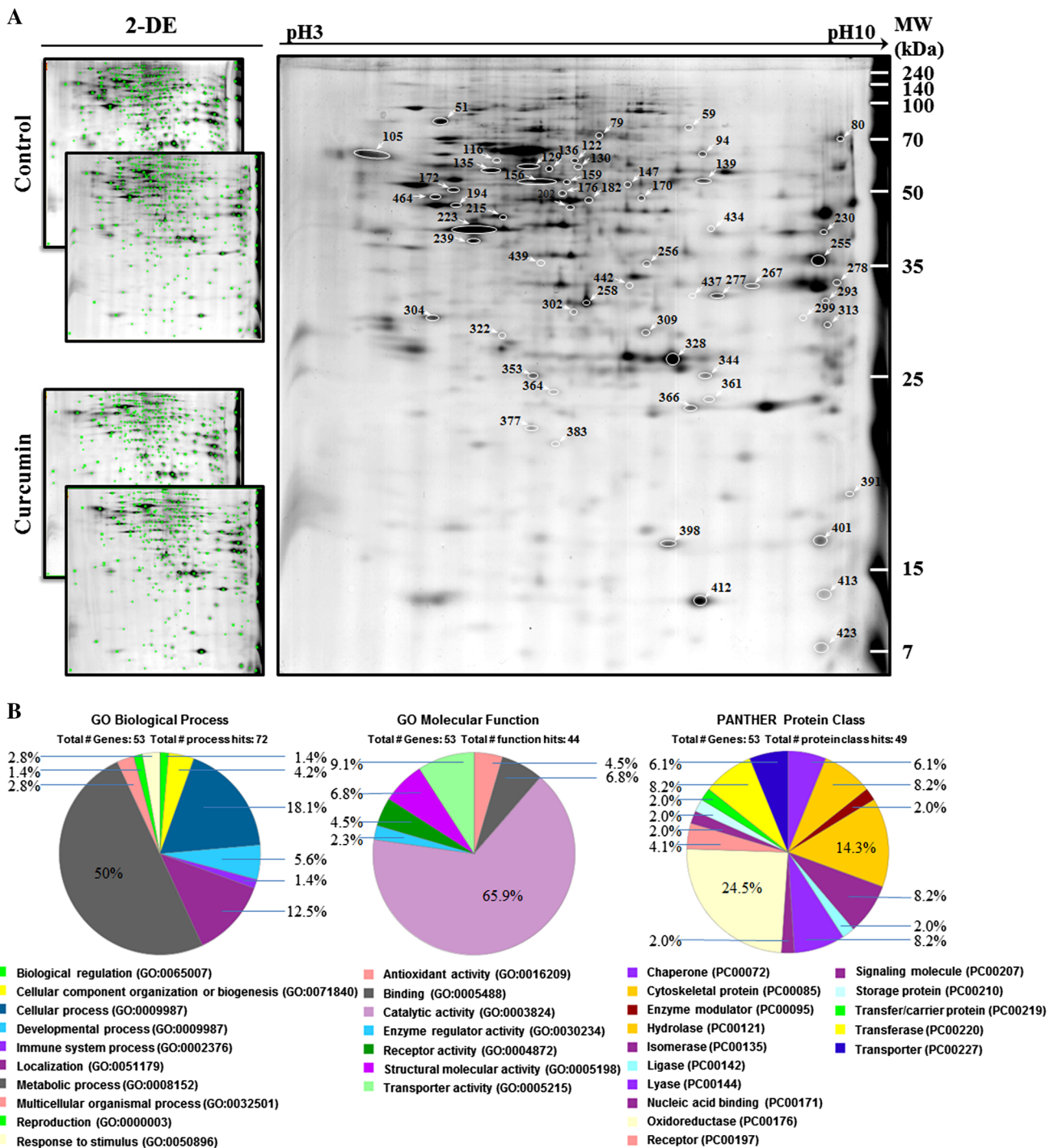
Fig. 1 Representative silver-stained 2-DE gel images of rat primary white adipocyte proteome. **a** Differentially regulated proteins and proteins of interest are marked with circles and arrows. The *numbers* in gels are listed in Table 1. **b** Fifty-eight identified proteins were classified into biological process, molecular function, and protein class using the PANTHER classification system

whereas ANXA2 was down-regulated. Based on these results, enhanced lipolysis mediated by increased HSL induction upon curcumin treatment affects lipid metabolism through alterations of adipose differentiation and adipose-derived hormone levels.

Validation network analysis using real-time RT-PCR

To evaluate the results of the DAVID classification, mitochondrial function-associated genes were further

Table 2 List of identified proteins showing differential expression in rat primary white adipocytes

Spot ID	Gene ID	UniProtKB	Description	Acc. No.[a]	Nominal mass (M_r)[b]	Calculated PI	Score[c]
51	Hsp90ab1	P34058	Heat shock protein 90 kDa alpha (cytosolic), class B member 1	gil51859516	83,631	4.97	170
59	Aco2	Q9ER34	Aconitate hydratase, mitochondrial precursor	gil40538860	86,121	7.87	195
79	Hpse	Q71RP1	Heparanase precursor	gil12018276	60,816	9.36	82
80	Hadha	Q64428	Trifunctional enzyme subunit alpha, mitochondrial precursor	gil148747393	83,297	9.16	135
94	Rab19	Q5M7U5	Ras-related protein Rab-19	RAB19_RAT	24,658	6.06	55
105	Emc3	Q5U2V8	ER membrane protein complex subunit 3	EMC3_RAT	29,960	6.33	52
116	Faah	P97612	Chain A, Crystal Structure Of Fatty Acid Amide Hydrolase Conjugated With The Drug-Like Inhibitor Pf-750	gil198443139	65,408	7.86	58
122	Dpysl2	P47942	Dihydropyrimidinase-related protein 2	DPYL2_RAT	62,638	5.95	100
129	Blvrb	B5DF65	PREDICTED: Flavin reductase (NADPH) isoform X1	gil672035614	13,504	6.69	69
130	Pgm1	Q499Q4	Phosphoglucomutase-1	gil77627971	61,637	6.14	112
135	Hspd1	P63039	Heat shock protein (hsp60) precursor	gil56383	61,098	5.91	180
136	Tcp1	P28480	T-complex protein 1 subunit alpha	gil6981642	60,835	5.86	111
139	Gpi	Q6P6V0	Glucose-6-phosphate isomerase	gil46485440	62,958	7.38	96
147	Dld	Q6P6R2	Dihydrolipoyl dehydrogenase, mitochondrial precursor	gil40786469	54,574	7.96	87
156	Pdia3	P11598	Protein disulfide-isomerase A3 precursor	gil8393322	57,010	5.88	175
159	Cct2	Q5XIM9	T-complex protein 1 subunit beta	gil54400730	57,764	6.01	99
170	Glud1	P10860	Glutamate dehydrogenase 1, mitochondrial precursor	gil6980956	61,719	8.05	170
172	Tuba1a	P68370	Tubulin, alpha 1A	gil38328248	50,816	4.94	131
176	Aldh2	P11884	Mitochondrial aldehyde dehydrogenase precursor	gil45737866	56,079	6.69	101
182	Eno1	P04764	Alpha-enolase	gil158186649	47,440	6.16	125
194	Atp5b	P10719	ATP synthase subunit beta, mitochondrial precursor	gil54792127	56,318	5.19	75
202	Eno1	P04764	Alpha-enolase	gil158186649	47,440	6.16	148
215	Gda	Q9JKB7	Guanine deaminase	gil148747414	51,439	5.48	143
223	Actb	P60711	Actin, cytoplasmic 1	ACTB_RAT	42,052	5.29	69
230	Acaa2	P13437	Acetyl-Coenzyme A acyltransferase 2 (mitochondrial 3-oxoacyl-Coenzyme A thiolase), isoform CRA_g	gil149027157	38,753	8.64	142
239	Actb	A1Z0K8	Beta-actin	gil119959830	31,955	5.24	75
255	Aldoa	P05065	Aldolase A	gil202837	39,691	8.31	149
256	Akr1a1	P51635	Alcohol dehydrogenase [NADP(+)]	gil13591894	36,711	6.84	139
258	Amotl2	A0A0G2KAV3	PREDICTED: Angiomotin-like protein 2 isoform X1	gil564365265	88,391	7.15	58
267	Gapdh	P04797	Glyceraldehyde-3-phosphate dehydrogenase	gil8393418	36,090	8.14	78
277	Anxa2	Q07936	Annexin A2	gil9845234	38,939	7.55	131
278	Mdh2	P04636	Malate dehydrogenase, mitochondrial precursor	gil42476181	36,117	8.93	122
293	Hnrnpa2b1	A7VJC2	Heterogeneous nuclear ribonucleoprotein A2	gil157059859	36,089	8.67	82
299	Vdac1	Q9Z2L0	Vdac1 protein, partial	gil38051979	32060	8.35	94
302	Gpd1	O35077	Glycerol-3-phosphate dehydrogenase [NAD(+)], cytoplasmic	gil57527919	38,112	6.16	94
304	Anxa5	P14668	Chain A, Rat Annexin V Crystal Structure: Ca2 + -Induced Conformational Changes	gil157836327	35,458	4.97	243
309	Cbr1	P47727	Carbonyl reductase [NADPH] 1	gil9506467	30,844	8.22	120
313	Lipe	P15304	Hormone-sensitive lipase, HSL (internal fragment)	gil386000	22,825	5.84	54

Table 2 continued

Spot ID	Gene ID	UniProtKB	Description	Acc. No.[a]	Nominal mass (M_r)[b]	Calculated PI	Score[c]
322	Gstm2	P08010	Glutathione S-transferase Mu 2	gil28933457	25,857	6.90	69
328	Car3	P14141	Carbonic anhydrase 3	gil31377484	29,698	6.89	149
344	Gstm2	P08010	Glutathione S-transferase Mu 2	gil28933457	25,857	6.90	72
353	Prdx6	O35244	Peroxiredoxin-6	gil16758348	24860	5.64	85
361	Gstp1	P04906	Glutathione S-transferase P	gil25453420	23,652	6.89	77
364	Prdx3	G3V7I0	Peroxiredoxin 3	gil149040547	28,567	7.14	88
366	Duox2	Q9ES45	Dual oxidase 2 short isoform	gil23664377	56,518	8.88	65
377	Rab1A	Q6NYB7	Ras-related protein Rab-1A	RAB1A_RAT	22,891	5.93	54
383	Atp5 h	P31399	ATP synthase subunit d, mitochondrial	gil9506411	18,809	6.17	142
391	Ppib	P24368	Peptidyl-prolyl cis–trans isomerase B precursor	gil11968126	22,845	9.42	124
398	Prdx5	Q9R063	Peroxiredoxin-5, mitochondrial precursor	gil16758404	22,507	8.94	96
401	Sorl1	Q9R0N2	LR11	gil6178000	8764	9.46	64
412	Fabp4	Q5XFV4	Fabp4 protein	gil54261546	14,841	7.74	73
413	Pfn1	P62963	Profilin	gil1628436	15,149	8.46	91
423	Hspe1	P26772	Chaperonin 10, cpn10	gil400542	10,764	8.91	87
434	Cs	Q8VHF5	Citrate synthase, mitochondrial precursor	gil18543177	52,176	8.53	91
437	Pcyox1	Q99ML5	Prenylcysteine oxidase 1, isoform CRA_b	gil149036615	48,930	5.96	55
439	Arfgef2	Q7TSU1	Brefeldin A-inhibited guanine nucleotide-exchange protein 2	BIG2_RAT	20,4297	6.08	52
442	Pde6b	D3ZDI8	Rod cGMP-specific 3′,5′-cyclic phosphodiesterase subunit beta	gil157822587	99,683	5.18	50
464	Tubb4b	Q6P9T8	Tubulin beta-4B chain	gil40018568	50,225	4.79	129

[a] NCBInr/SWISS database accession number

[b] The nominal mass is the integer mass of the most abundant naturally occurring stable isotope of an element

[c] MASCOT probability-based molecular-weight search score calculated for PMF. Protein score is—$10\times \log(p)$, where p is the probability that the observed match is a random event; it is based on the NCBInr database using the MASCOT searching program as MS/MS data. Protein scores >61 are significant ($p < 0.05$). Spot ID is same number in gel image of Fig. 1

confirmed using real-time RT-PCR (Fig. 4b). Among the mitochondrial protein-coding genes in adipocytes, ten protein-coding genes (*Acaa2*, *Atp5b*, *Atp5 h*, *Cs*, *Gpd*, *Hadha*, *Hspd1*, *Hspe1*, *Mdh2*, and *Vdac1*) were selected from the list of identified candidates by DAVID. Their mRNA levels were significantly altered, and expression patterns of all genes were in line with the proteomic results. Moreover, curcumin treatment led to significant elevation of mitochondrial *Acaa2* and *Hadha* levels, suggesting enhanced fatty acid degradation in mitochondria.

To confirm the activities of key browning and thermogenic markers together with other mitochondrial proteins, we measured expression levels of *Ucp1*, *Ucp2*, *Ucp3*, and *Ppard* in response to curcumin treatment (Fig. 4c). As expected, higher mRNA expression of *Ucp1* was observed in curcumin-treated adipocytes compared with control cells, whereas *Ppard* expression was not significantly changed by curcumin treatment. This result suggests that curcumin dissipates energy as heat by uncoupling the mitochondrial respiratory chain from ATP formation through expression of *Ucp1*.

Interactions of browning markers in primary white adipocytes

To understand interactions between the identified proteins and brown fat-specific markers in primary white adipocytes, six important browning markers (*Cebpb*, *Prkaa2*, *Ppargc1a*, *Pparg*, *Prdm16*, and *Ucp1*) were subjected to functional analysis using STRING network analysis. The network analysis results revealed possible interactions between the identified proteins and brown fat-specific markers (Fig. 5). Combined results from the proteomic and network analysis identified eight genes as protein-coding genes, and two candidates (HSL/*Lipe* and FABP4/*Fabp4*) showed possible interactions with six browning markers (zoom in image in Fig. 5). These results suggest that two candidates (HSL and FABP4) associated with UCP1 play
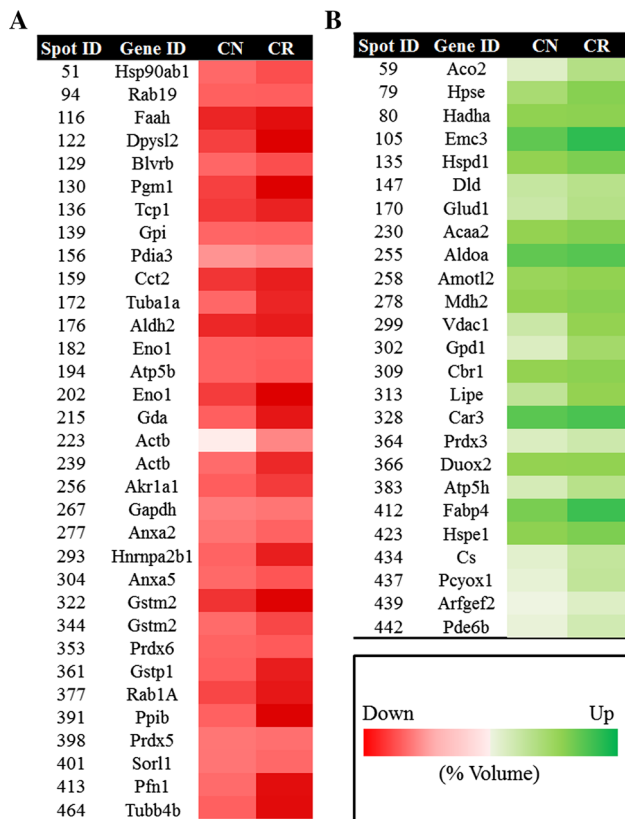
A

Spot ID	Gene ID	CN	CR
51	Hsp90ab1		
94	Rab19		
116	Faah		
122	Dpysl2		
129	Blvrb		
130	Pgm1		
136	Tcp1		
139	Gpi		
156	Pdia3		
159	Cct2		
172	Tuba1a		
176	Aldh2		
182	Eno1		
194	Atp5b		
202	Eno1		
215	Gda		
223	Actb		
239	Actb		
256	Akr1a1		
267	Gapdh		
277	Anxa2		
293	Hnrnpa2b1		
304	Anxa5		
322	Gstm2		
344	Gstm2		
353	Prdx6		
361	Gstp1		
377	Rab1A		
391	Ppib		
398	Prdx5		
401	Sorl1		
413	Pfn1		
464	Tubb4b		

B

Spot ID	Gene ID	CN	CR
59	Aco2		
79	Hpse		
80	Hadha		
105	Emc3		
135	Hspd1		
147	Dld		
170	Glud1		
230	Acaa2		
255	Aldoa		
258	Amotl2		
278	Mdh2		
299	Vdac1		
302	Gpd1		
309	Cbr1		
313	Lipe		
328	Car3		
364	Prdx3		
366	Duox2		
383	Atp5h		
412	Fabp4		
423	Hspe1		
434	Cs		
437	Pcyox1		
439	Arfgef2		
442	Pde6b		

Down   Up

(% Volume)

Fig. 2 Differentially regulated proteins in rat primary white adipocytes from curcumin-treated (CR) group compared with control (CN) group. **a** Down-regulated and **b** Up-regulated proteins. Each *bar* shows an average volume density (%) in 2-DE analysis. Statistical significances between control and curcumin-treated groups were determined by One-way ANOVA test, where $p < 0.05$

significant roles in controlling the browning phenotype in white adipocytes.

Validation of browning marker interactions in rat primary adipocytes

Interestingly, STRING network analysis revealed interactions between HSL (*Lipe*) and main browning players. To validate these results, six protein-coding genes (*Cebpb*, *Fabp4*, *Lipe*, *Pparg*, *Ppargc1a*, and *Prdm16*) were selected for further real-time PCR analysis. Expression levels of three protein-coding genes (*Fabp4*, *Lipe*, and *Pparg*) were significantly up-regulated (16, 8, and 7-fold changes, respectively) by curcumin treatment in primary white adipocytes (Fig. 6a). Furthermore, to verify interaction targets, HSL (*Lipe*) was immunoprecipitated with primary adipocyte lysates from each group (Fig. 6b) and validated further by Western blotting. The results show that UCP1 and PGC-1α were co-expressed with AMPK, C/EBPβ, HSL, and PPARγ. Interestingly, four interacting proteins (AMPK, C/EBPβ, HSL, and PPARγ) were up-regulated

along with UCP1 expression by curcumin treatment, whereas these four proteins were down-regulated with PGC-1α expression. These data suggest that HSL is concomitantly expressed along with UCP1 during fuel metabolism and trans-differentiation from white to brown adipocytes during adipocyte differentiation. Interaction of UCP1 and HSL was further validated in primary white adipocytes by dual-fluorescent staining (Fig. 6c).

Discussion

In this proteome study, we observed differential expression of multiple proteins involved in mitochondrial function in primary white adipocytes upon curcumin treatment, suggesting enhanced fatty acid oxidation and mitochondrial biogenesis. To further investigate the roles of the identified proteins in primary white adipocytes, we performed analyses using the PANTHER, DAVID, and STRING databases. Interestingly, our proteomic results revealed differential expression of multiple proteins involved in lipid metabolism and mitochondrial function.

A recent study by Wang et al. [33] demonstrated that curcumin can potentially prevent obesity by inducing browning of inguinal WAT via the norepinephrine-β3AR pathway. Consistent with these data, we found that curcumin significantly elevated expression of brown fat-specific markers (*Tmem26* and *Tbx1*) as well as proteins such as UCP1, PGC-1α, and PRDM16 [19]. Taken together, these findings suggest that curcumin plays a dual modulatory role in inhibition of adipogenesis as well as induction of the brown fat-like phenotype. However, these recent studies have not been able to identify correlations between brite-specific markers and other browning-associated proteins in WAT via promotion of WAT remodeling in response to curcumin treatment.

Our results show that curcumin obviously elevated expression of proteins/genes involved in both fatty acid oxidation and the TCA cycle, which may contribute to reduced adiposity. Two (CS and HADHA) out of 14 mitochondrial proteins in primary white adipocytes showed higher expression upon curcumin treatment. CS is a Krebs TCA cycle enzyme that catalyzes synthesis of citrate from oxaloacetate and acetyl coenzyme A. HADHA catalyzes the last three steps of mitochondrial β-oxidation of long-chain fatty acids and plays important roles in control and regulation of β-oxidation [34]. In addition, partial inhibition of fatty acid oxidation has been reported as a therapy for non-insulin dependent diabetes mellitus (NIDDM) [35]. A recent study found that these two proteins show reduced mitochondrial expression in human omental fat from obese subjects and are directly involved in energy metabolism of cells [36, 37]. ACAA2 is also involved in the fatty acid

A

| Annotation Cluster 1	Enrichment Score: 7.95			Count	P_Value	Benjamini	FDR
GOTERM_CC_FAT	mitochondrial lumen	RT		12	1.6E-10	2.5E-8	1.9E-7
GOTERM_CC_FAT	mitochondrial matrix	RT		12	1.6E-10	2.5E-8	1.9E-7
SP_PIR_KEYWORDS	mitochondrion	RT		14	4.3E-7	3.2E-5	5.1E-4
GOTERM_CC_FAT	mitochondrial part	RT		13	1.4E-6	5.5E-5	1.7E-3
Annotation Cluster 2	**Enrichment Score: 4.58**			**Count**	**P_Value**	**Benjamini**	**FDR**
GOTERM_BP_FAT	alcohol catabolic process	RT		6	8.2E-6	1.4E-3	1.2E-2
GOTERM_BP_FAT	cellular carbohydrate catabolic process	RT		6	8.2E-6	1.4E-3	1.2E-2
GOTERM_BP_FAT	monosaccharide metabolic process	RT		8	2.7E-5	3.1E-3	4.1E-2
GOTERM_BP_FAT	glucose metabolic process	RT		7	5.7E-5	5.7E-3	8.6E-2
GOTERM_BP_FAT	hexose metabolic process	RT		7	1.3E-4	7.3E-3	1.9E-1
Annotation Cluster 3	**Enrichment Score: 4.48**			**Count**	**P_Value**	**Benjamini**	**FDR**
GOTERM_BP_FAT	carbohydrate catabolic process	RT		7	2.0E-6	6.9E-4	3.0E-3
GOTERM_BP_FAT	alcohol catabolic process	RT		6	8.2E-6	1.4E-3	1.2E-2
GOTERM_BP_FAT	cellular carbohydrate catabolic process	RT		6	8.2E-6	1.4E-3	1.2E-2
GOTERM_BP_FAT	glycolysis	RT		5	2.7E-5	3.7E-3	4.0E-2
GOTERM_BP_FAT	glucose catabolic process	RT		5	6.8E-5	5.9E-3	1.0E-1
GOTERM_BP_FAT	hexose catabolic process	RT		5	7.8E-5	6.0E-3	1.2E-1
GOTERM_BP_FAT	monosaccharide catabolic process	RT		5	7.8E-5	6.0E-3	1.2E-1
SP_PIR_KEYWORDS	glycolysis	RT		4	9.0E-4	1.3E-2	1.1E0

B
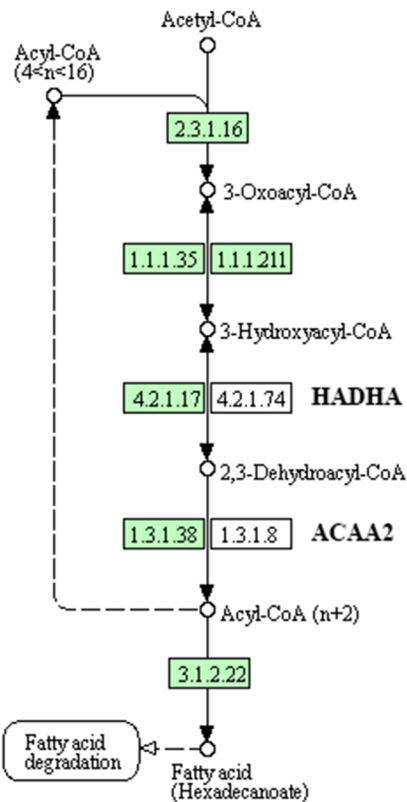
Fig. 3 Discovery enriched functional-related gene groups from differentially regulated proteins between control (CN) and curcumin-treated (CR) groups. **a** Functional classification by DAVID and **b** protein pathway in KEGG pathway
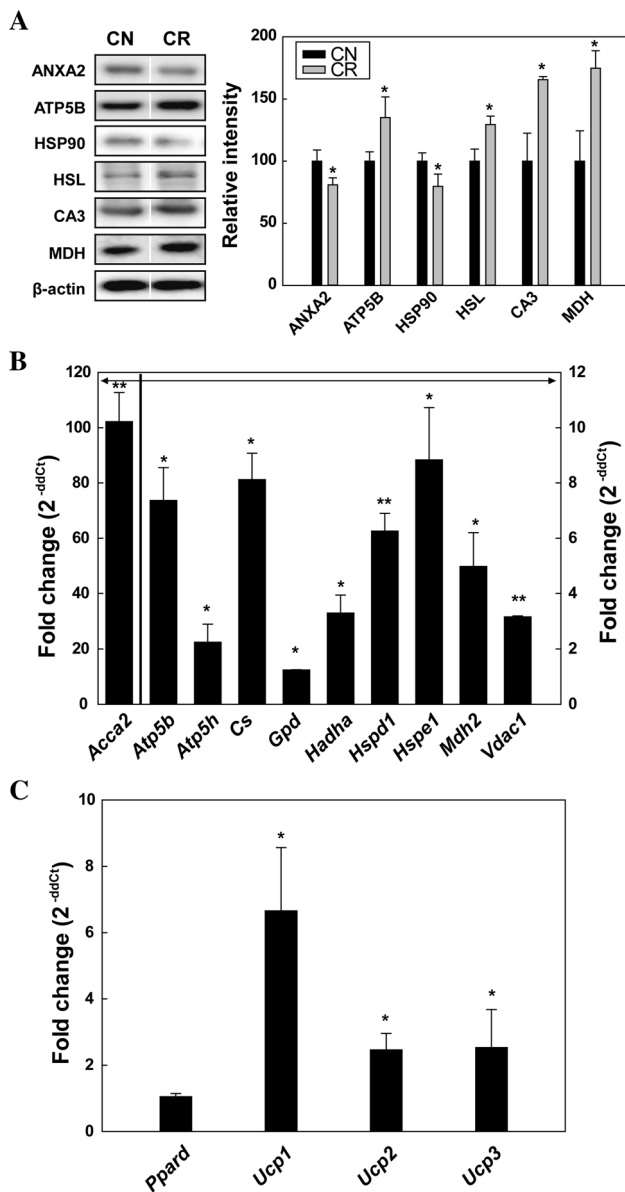
Fig. 4 Validation of fatty acid metabolism and mitochondrial proteins by Western blotting. **a** mRNA expression levels of mitochondrial protein-coding genes **b** and thermogenesis genes by real-time PCR **c** in control (CN) and curcumin-treated (CR) groups. Real-time PCR and immunoblot analysis results are expressed as relative intensity normalized to *Gapdh*/β-actin and represent the mean ± S.E.M of triplicate independent experiments. Statistical significance was determined by one-way ANOVA test, where $*p < 0.05$ and $**p < 0.01$. Relative changes in gene expression were quantified using the $\Delta\Delta C_T$ method. Fold changes refer to expression ratios of CR to CN

metabolism pathway and catalyzes the last step of the mitochondrial fatty acid β-oxidation pathway [38]. Our data support an increased number of mitochondria and dramatically increased expression of ACAA2/*Acaa2*, which also activates mitochondrial fatty acid β-oxidation.

ATP synthase is localized to the plasma membrane in many different cell types, including endothelial cells and adipocytes, and they may contribute to regulation of lipid metabolism and cellular proliferation [39]. Although the function of the *ATP5B* gene product is not clear, reduced expression of the *ATP5B* gene was detected in various types of human tumors [40]. Catalytic sites of ATP synthesis are present in the β subunit, which plays a crucial role in energy metabolism and directly participates in energy production. According to our findings, ATP5B presumably contributes to mitochondrial oxidative phosphorylation and mitochondrial biogenesis.

It is well known that two essential malate dehydrogenases, MDH1 (cytosolic malate dehydrogenase) and MDH2 (mitochondrial malate dehydrogenase), play important roles in the Krebs cycle for energy metabolism. The native dimeric form of this enzyme is specifically activated by citrate in the NAD + leads to NADH direction and inhibited by citrate in the NADH leads to NAD + direction [41]. Furthermore, Zou et al. [42] reported that breed-, gender-, and tissue-specific expression patterns of *Mdh2* expression are positively correlated with adipocyte volume across six adipose tissue types. We observed consistent up-regulation of MDH/*Mdh2* in primary white adipocytes by curcumin treatment. Interestingly, a recent report highlighted the role of lactate in energy metabolism and revealed an effect on WAT browning [43]. Induction of *Ucp1* by an increased redox state (NADH, H^+-to-NAD^+) favors its dissipation through increased uncoupled respiration. Browning of white adipocytes by intermediate metabolites constitutes an adaptive mechanism to alleviate redox pressure. Further study is needed to fully understand the mechanism and to further determine whether or not this browning mechanism plays a significant role in energy expenditure.

Fatty acids must be esterified to Coenzyme A before they can undergo oxidative degradation, and two major lipases (ATGL and HSL) are involved in lipid degradation. Activation of HSL in adipocytes has been proposed to play an essential role in the regulation of body weight and fat mass since HSL is responsible for release of FFA from stored TG in adipose tissues [44, 45]. In contrast to our expectations, it was suggested that mice lacking HSL expend more energy during thermogenesis than control mice [44]. Furthermore, it was also reported that the fasting-induced loss of body weight is correlated with UCP2 expression but not UCP1 expression in BAT [44]. However, we observed that enhanced lipolysis mediated by increased HSL induction upon curcumin treatment affected lipid metabolism through alterations of adipose differentiation and adipose-derived hormone levels. In addition, curcumin treatment led to increased expression of FABP4, which might promote binding to newly released fatty acids [46]. Our results suggest that HSL is probably involved in the determination of white versus brown adipocytes during
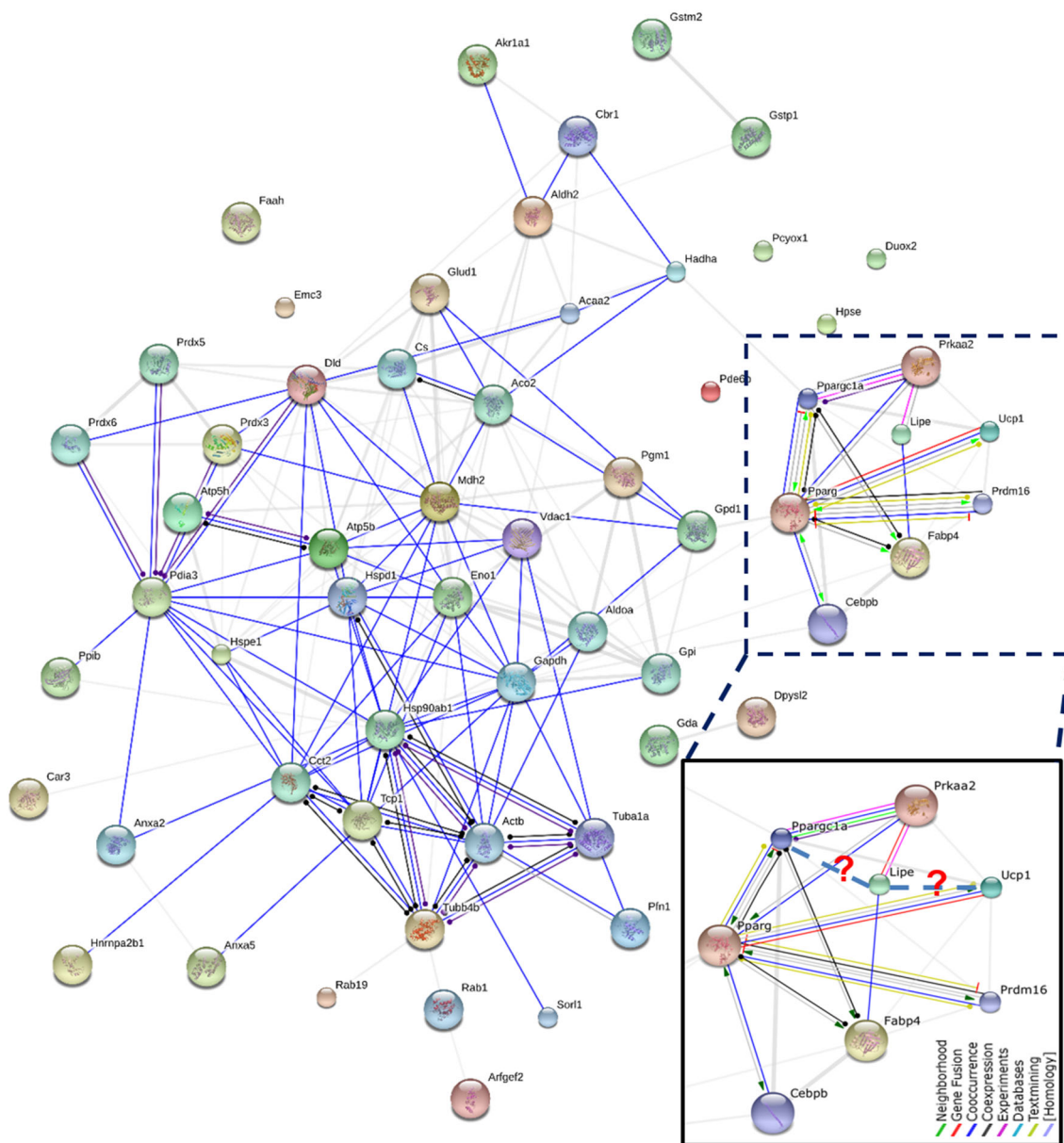
Fig. 5 Discovery of novel fat-browning markers by network analysis from differentially regulated proteins in response to curcumin treatment. Interaction of identified proteins with main fat-browning *markers* using the web-based software tool STRING as well as two proteins (FABP4, HSL (LIPE)) highly connected with six fat-browning markers in STRING. Zoom in image (*red* question *markers*) shows that HSL is tightly connected with two proteins (PGC-1α and UCP1). (Color figure online)

adipocyte differentiation, which was in line with earlier result reported by other investigators [47]. Although the exact mechanisms underlying this novel role of HSL remain to be elucidated, it seems clear that HSL is, at least in part, participates in the control of browning of white adipocytes.

The multifunctional protein ANXA2 is down-regulated after exercise or diet intervention in human adipose tissue, and it has been suggested to enhance GLUT4 translocation to membranes [48]. Our recent study found that thiodigalactocide (TDG) binding to galectin 1 (GAL1) may restrict formation of the GAL1-ANXA2-VIM (vimentin) interactome, as these proteins were all down-regulated, leading to lower lipid droplet formation [49]. Down-regulation of ANXA2 and VIM together with GAL1 led to reduced lipogenesis or TG synthesis in TDG-treated rats. These findings suggest that curcumin plays a modulatory role in inhibition of adipogenesis as well as transformation of lipid droplets via alteration of lipid droplet-associated proteins in primary white adipocytes. In summary, the molecular mechanisms underlying curcumin-induced increased differentiation of primary white adipocytes seem
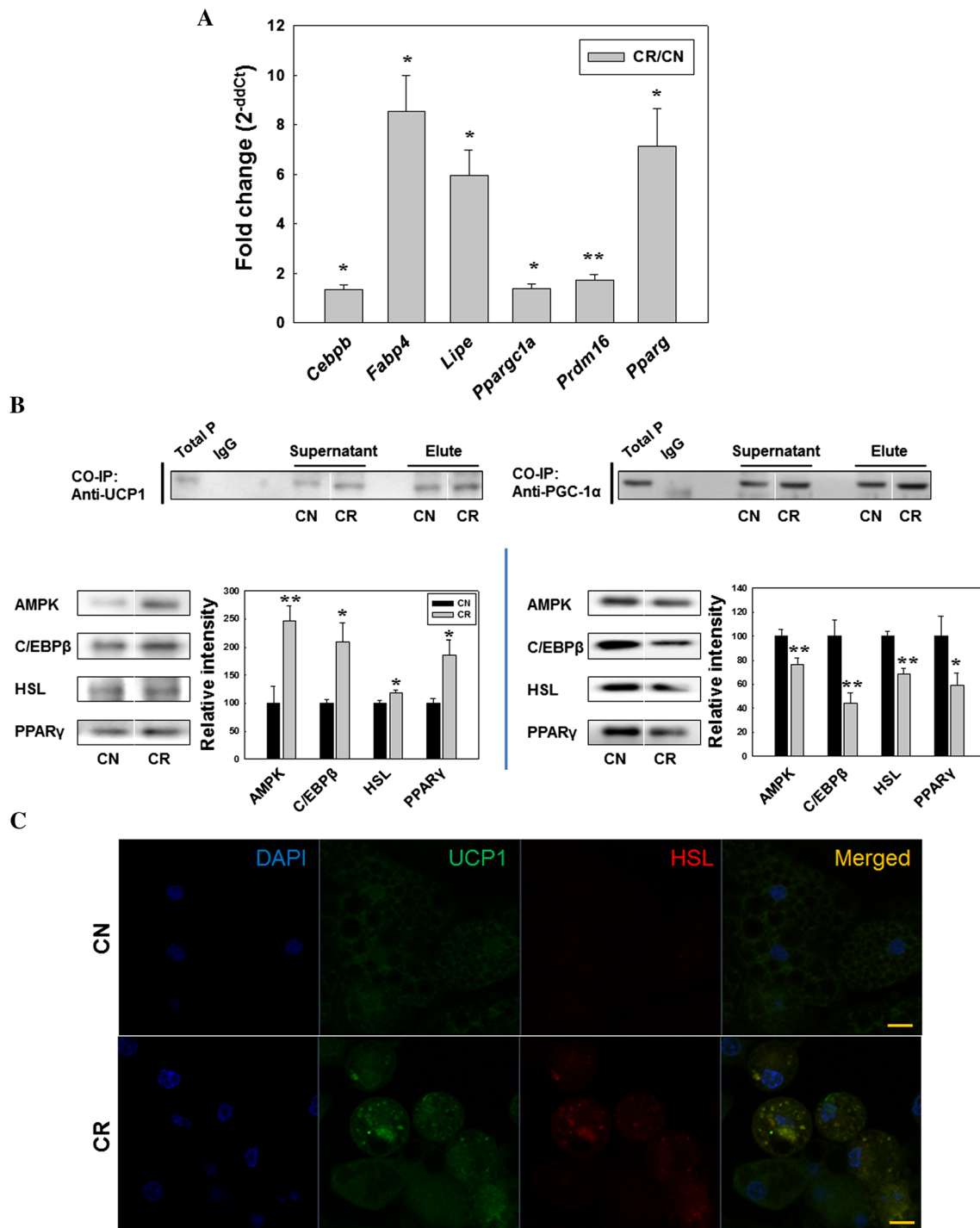
Fig. 6 Validation of proteomic data and predicted targets generated by network analysis. **a** Real-time RT-PCR, **b** interaction of PGC-1α, UCP1, and HSL validated by co-immunoprecipitation-based Western blot analysis, and **c** co-localization of UCP1 and HSL in rat primary white adipocytes. Real-time PCR and immunoblot analysis results are expressed as relative intensity normalized to *Gapdh*/β-actin and represent the mean ± S.E.M of triplicate independent experiments. Statistical significance was determined by one-way ANOVA test, where *$p < 0.05$ and **$p < 0.01$

to involve induction of increased fatty acid metabolism by ACAA2. Additionally, translocation of HSL to lipid droplets is the critical event regulating lipolysis induced by

curcumin treatment. These FA are used by mitochondria, as demonstrated by increased expression of enzymes involved in β-oxidation and mitochondrial biogenesis (ATP5B,
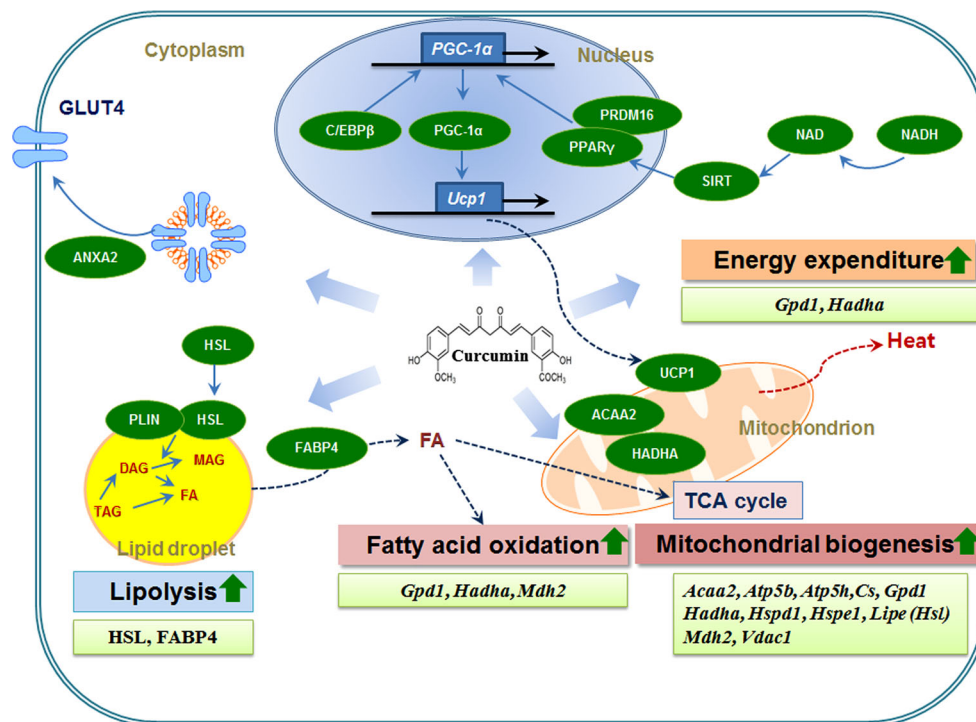
Fig. 7 Proposed schematic diagram of differentially regulated proteins/genes determining curcumin-induced browning in rat primary white adipocytes. For abbreviated protein names, see Abbreviations and Table 2. (*Arrow*) *stimulatory*, (*dashed line*) *translocation*, (*up arrow*) *up-regulation*

ACAA2, and HADHA). Enhanced FA utilization induces production of acetyl-CoA as well as a proton gradient between the two mitochondrial membranes. This gradient is dissipated by UCP1, thereby increasing heat production in primary white adipocytes upon curcumin treatment. ANXA2 is down-regulated after curcumin treatment and has been shown to enhance GLUT4 translocation to membranes. These results suggest that curcumin plays a modulatory role in inhibition of adipogenesis and lipogenesis by increasing protein levels associated with lipolysis, fatty acid β-oxidation, and energy expenditure (Fig. 7).

In conclusion, curcumin promotes fatty acid oxidation, mitochondrial activity, and Ucp1 expression possibly by activating a regulator of mitochondrial function. Finally, we systematically identified candidates involved in lipolysis, fatty acid β-oxidation, and energy expenditure.

Compliance with ethical standards

Conflict of interest The authors have declared no conflict of interest.

References

1. Haslam DW, James WP (2005) Obesity. Lancet 366:1197–1209
2. Tonstad S, Despres JP (2011) Treatment of lipid disorders in obesity. Expert Rev Cardiovasc Ther 9:1069–1080
3. Chang J, Oikawa S, Iwahashi H, Kitagawa E, Takeuchi I, Yuda M, Aoki C, Yamada Y, Ichihara G, Kato M, Ichihara S (2014) Expression of proteins associated with adipocyte lipolysis was significantly changed in the adipose tissues of the obese spontaneously hypertensive/NDmcr-cp rat. Diabetol Metab Syndr 6:8
4. Noreldin AA, Abd Elhamid AM, Hashem AM, Afifi AM (2013) A pilot study on the use of injection lipolysis in visceral adipose tissues. Aesthet Surg J 33:431–435
5. Mercer SW, Williamson DH (1988) The influence of starvation and natural refeeding on the rate of triacylglycerol/fatty acid substrate cycling in brown adipose tissue and different white adipose sites of the rat in vivo. The role of insulin and the sympathetic nervous system. Biosci Rep 8:147–153
6. Ricquier D (1998) Neonatal brown adipose tissue, UCP1 and the novel uncoupling proteins. Biochem Soc Trans 26:120–123
7. Galmozzi A, Sonne SB, Altshuler-Keylin S, Hasegawa Y, Shinoda K, Luijten IH, Chang JW, Sharp LZ, Cravatt BF, Saez E, Kajimura S (2014) ThermoMouse: an in vivo model to identify modulators of UCP1 expression in brown adipose tissue. Cell Rep 9:1584–1593
8. Reddy NL, Jones TA, Wayte SC, Adesanya O, Sankar S, Yeo YC, Tripathi G, McTernan PG, Randeva HS, Kumar S, Hutchinson CE, Barber TM (2014) Identification of brown adipose tissue using MR imaging in a human adult with histological and immunohistochemical confirmation. J Clin Endocrinol Metab 99:E117–E121

9. Harms M, Seale P (2013) Brown and beige fat: development, function and therapeutic potential. Nat Med 19:1252–1263

10. Cohen P, Spiegelman BM (2015) Brown and beige fat: molecular parts of a thermogenic machine. Diabetes 64:2346–2351

11. Yoshitomi H, Yamazaki K, Abe S, Tanaka I (1998) Differential regulation of mouse uncoupling proteins among brown adipose tissue, white adipose tissue, and skeletal muscle in chronic beta 3 adrenergic receptor agonist treatment. Biochem Biophys Res Commun 253:85–91

12. Mulligan JD, Gonzalez AA, Stewart AM, Carey HV, Saupe KW (2007) Upregulation of AMPK during cold exposure occurs via distinct mechanisms in brown and white adipose tissue of the mouse. J Physiol 580:677–684

13. Bonet ML, Oliver P, Palou A (2013) Pharmacological and nutritional agents promoting browning of white adipose tissue. Biochim Biophys Acta 1831:969–985

14. Baboota RK, Singh DP, Sarma SM, Kaur J, Sandhir R, Boparai RK, Kondepudi KK, Bishnoi M (2014) Capsaicin induces "brite" phenotype in differentiating 3T3-L1 preadipocytes. Plos One 9:e103093

15. Zhang Z, Zhang H, Li B, Meng X, Wang J, Zhang Y, Yao S, Ma Q, Jin L, Yang J, Wang W, Ning G (2014) Berberine activates thermogenesis in white and brown adipose tissue. Nat Commun 5:5493

16. Sellayah D, Bharaj P, Sikder D (2011) Orexin is required for brown adipose tissue development, differentiation, and function. Cell Metab 14:478–490

17. Shishodia S, Sethi G, Aggarwal BB (2005) Curcumin: getting back to the roots. Ann N Y Acad Sci 1056:206–217

18. Shehzad A, Ha T, Subhan F, Lee YS (2011) New mechanisms and the anti-inflammatory role of curcumin in obesity and obesity-related metabolic diseases. Eur J Nutr 50:151–161

19. Lone J, Choi JH, Kim SW, Yun JW (2016) Curcumin induces brown fat-like phenotype in 3T3-L1 and primary white adipocytes. J Nutr Biochem 27:193–202

20. Joo JI, Oh TS, Kim DH, Choi DK, Wang X, Choi JW, Yun JW (2011) Differential expression of adipose tissue proteins between obesity-susceptible and -resistant rats fed a high-fat diet. Proteomics 11:1429–1448

21. Forner F, Kumar C, Luber CA, Fromme T, Klingenspor M, Mann M (2009) Proteome differences between brown and white fat mitochondria reveal specialized metabolic functions. Cell Metab 10:324–335

22. Kamal AH, Kim WK, Cho K, Park A, Min JK, Han BS, Park SG, Lee SC, Bae KH (2013) Investigation of adipocyte proteome during the differentiation of brown preadipocytes. J Proteomics 94:327–336

23. Birner-Gruenberger R, Susani-Etzerodt H, Waldhuber M, Riesenhuber G, Schmidinger H, Rechberger G, Kollroser M, Strauss JG, Lass A, Zimmermann R, Haemmerle G, Zechner R, Hermetter A (2005) The lipolytic proteome of mouse adipose tissue. Mol Cell Proteomics 4:1710–1717

24. Okita N, Hayashida Y, Kojima Y, Fukushima M, Yuguchi K, Mikami K, Yamauchi A, Watanabe K, Noguchi M, Nakamura M, Toda T, Higami Y (2012) Differential responses of white adipose tissue and brown adipose tissue to caloric restriction in rats. Mech Ageing Dev 133:255–266

25. Rodeheffer MS, Birsoy K, Friedman JM (2008) Identification of white adipocyte progenitor cells in vivo. Cell 135:240–249

26. Kim CY, Le TT, Chen C, Cheng JX, Kim KH (2011) Curcumin inhibits adipocyte differentiation through modulation of mitotic clonal expansion. J Nutr Biochem 22:910–920

27. Choi DK, Oh TS, Choi JW, Mukherjee R, Wang X, Liu H, Yun JW (2011) Gender difference in proteome of brown adipose tissues between male and female rats exposed to a high fat diet. Cell Physiol Biochem 28:933–948

28. Kim SW, Park TJ, Choi JH, Aseer KR, Choi JY, Kim YJ, Choi MS, Yun JW (2015) Differential protein expression in white adipose tissue from obesity-prone and obesity-resistant mice in response to high fat diet and anti-obesity herbal medicines. Cell Physiol Biochem 35:1482–1498

29. Mi H, Muruganujan A, Casagrande JT, Thomas PD (2013) Large-scale gene function analysis with the PANTHER classification system. Nat Protoc 8:1551–1566

30. da Huang W, Sherman BT, Lempicki RA (2009) Systematic and integrative analysis of large gene lists using DAVID bioinformatics resources. Nat Protoc 4:44–57

31. Livak KJ, Schmittgen TD (2001) Analysis of relative gene expression data using real-time quantitative PCR and the 2(-delta delta C(T)) method. Methods 25:402–408

32. Chaudhari HN, Kim SW, Yun JW (2015) Gender-dimorphic regulation of DJ1 and its interactions with metabolic proteins in streptozotocin-induced diabetic rats. J Cell Mol Med 19:996–1009

33. Wang S, Wang X, Ye Z, Xu C, Zhang M, Ruan B, Wei M, Jiang Y, Zhang Y, Wang L, Lei X, Lu Z (2015) Curcumin promotes browning of white adipose tissue in a norepinephrine-dependent way. Biochem Biophys Res Commun 466:247–253

34. Liu X, Wu L, Deng G, Li N, Chu X, Guo F, Li D (2008) Characterization of mitochondrial trifunctional protein and its inactivation study for medicine development. Biochim Biophys Acta 1784:1742–1749

35. Foley JE (1992) Rationale and application of fatty acid oxidation inhibitors in treatment of diabetes mellitus. Diabetes Care 15:773–784

36. Perez-Perez R, Garcia-Santos E, Ortega-Delgado FJ, Lopez JA, Camafeita E, Ricart W, Fernandez-Real JM, Peral B (2012) Attenuated metabolism is a hallmark of obesity as revealed by comparative proteomic analysis of human omental adipose tissue. J Proteomics 75:783–795

37. Lindinger PW, Christe M, Eberle AN, Kern B, Peterli R, Peters T, Jayawardene KJ, Fearnley IM, Walker JE (2015) Important mitochondrial proteins in human omental adipose tissue show reduced expression in obesity. J Proteomics 124:79–87

38. Abe H, Ohtake A, Yamamoto S, Satoh Y, Takayanagi M, Amaya Y, Takiguchi M, Sakuraba H, Suzuki Y, Mori M et al (1993) Cloning and sequence analysis of a full length cDNA encoding human mitochondrial 3-oxoacyl-CoA thiolase. Biochim Biophys Acta 1216:304–306

39. Kim KB, Lee JW, Lee CS, Kim BW, Choo HJ, Jung SY, Chi SG, Yoon YS, Yoon G, Ko YG (2006) Oxidation-reduction respiratory chains and ATP synthase complex are localized in detergent-resistant lipid rafts. Proteomics 6:2444–2453

40. Geyik E, Igci YZ, Pala E, Suner A, Borazan E, Bozgeyik I, Bayraktar E, Bayraktar R, Ergun S, Cakmak EA, Gokalp A, Arslan A (2014) Investigation of the association between ATP2B4 and ATP5B genes with colorectal cancer. Gene 540:178–182

41. McEvily AJ, Mullinax TR, Dulin DR, Harrison JH (1985) Regulation of mitochondrial malate dehydrogenase: kinetic modulation independent of subunit interaction. Arch Biochem Biophys 238:229–236

42. Zhou SL, Li MZ, Li QH, Guan JQ, Li XW (2012) Differential expression analysis of porcine MDH1, MDH2 and ME1 genes in adipose tissues. Genet Mol Res 11:1254–1259

43. Carriere A, Jeanson Y, Berger-Muller S, Andre M, Chenouard V, Arnaud E, Barreau C, Walther R, Galinier A, Wdziekonski B, Villageois P, Louche K, Collas P, Moro C, Dani C, Villarroya F, Casteilla L (2014) Browning of white adipose cells by intermediate metabolites: an adaptive mechanism to alleviate redox pressure. Diabetes 63:3253–3265

44. Harada K, Shen WJ, Patel S, Natu V, Wang J, Osuga J, Ishibashi S, Kraemer FB (2003) Resistance to high-fat diet-induced obesity

and altered expression of adipose-specific genes in HSL-deficient mice. Am J Physiol Endocrinol Metab 285:E1182–E1195

45. Holm C, Osterlund T, Laurell H, Contreras JA (2000) Molecular mechanisms regulating hormone-sensitive lipase and lipolysis. Annu Rev Nutr 20:365–393

46. Bouwman FG, Wang P, van Baak M, Saris WH, Mariman EC (2014) Increased beta-oxidation with improved glucose uptake capacity in adipose tissue from obese after weight loss and maintenance. Obesity (Silver Spring) 22:819–827

47. Strom K, Hansson O, Lucas S, Nevsten P, Fernandez C, Klint C, Moverare-Skrtic S, Sundler F, Ohlsson C, Holm C (2008)

Attainment of brown adipocyte features in white adipocytes of hormone-sensitive lipase null mice. Plos One 3:e1793

48. Leggate M, Carter WG, Evans MJ, Vennard RA, Nimmo MA, Sribala-Sundaram S (1985) Determination of inflammatory and prominent proteomic changes in plasma and adipose tissue after high-intensity intermittent training in overweight and obese males. J Appl Physiol 112:1353–1360

49. Mukherjee R, Kim SW, Park T, Choi MS, Yun JW (2015) Targeted inhibition of galectin 1 by thiodigalactoside dramatically reduces body weight gain in diet-induced obese rats. Int J Obes (Lond) 39:1349–1358